A Structural and Functional Assessment of the Lung via Multidetector-Row Computed Tomography

Phenotyping Chronic Obstructive Pulmonary Disease

Eric A. Hoffman, Brett A. Simon, and Geoffrey McLennan

Departments of Radiology, Medicine, and Biomedical Engineering, University of Iowa, Iowa City, Iowa; and Department of Anesthesiology and Critical Care Medicine, Johns Hopkins University, Baltimore, Maryland

With advances in multidetector-row computed tomography (MDCT), it is now possible to image the lung in 10 s or less and accurately extract the lungs, lobes, and airway tree to the fifth- through seventh-generation bronchi and to regionally characterize lung density, texture, ventilation, and perfusion. These methods are now being used to phenotype the lung in health and disease and to gain insights into the etiology of pathologic processes. This article outlines the application of these methodologies with specific emphasis on chronic obstructive pulmonary disease. We demonstrate the use of our methods for assessing regional ventilation and perfusion and demonstrate early data that show, in a sheep model, a regionally intact hypoxic pulmonary vasoconstrictor (HPV) response with an apparent inhibition of HPV regionally in the presence of inflammation. We present the hypothesis that, in subjects with pulmonary emphysema, one major contributing factor leading to parenchymal destruction is the lack of a regional blunting of HPV when the regional hypoxia is related to regional inflammatory events (bronchiolitis or alveolar flooding). If maintaining adequate blood flow to inflamed lung regions is critical to the nondestructive resolution of inflammatory events, the pathologic condition whereby HPV is sustained in regions of inflammation would likely have its greatest effect in the lung apices where blood flow is already reduced in the upright body posture.

Keywords: airways; computed tomography; emphysema; inflammation; functional imaging

The goal of this article reflects that of the mandate for guest speakers at the Aspen Lung Conference: to provide a state-of-the-art overview and to introduce a new and possibly controversial hypothesis. The focus of the conference was chronic obstructive pulmonary disease (COPD), and the goal of this article is to introduce the breadth of tools now available through advanced multidetector-row computed tomography (MDCT) that can be used to gain new insights into lung pathologies associated with COPD.

The pathologic events leading to emphysema are insidious and include structural and physiologic alterations that are characterized by inflammatory processes within the peripheral pulmonary parenchyma, thickening of arteriolar walls, and parenchymal destruction. A growing body of literature documents that these changes are likely to be associated with alterations in blood flow dynamics at a regional, microvascular level, and thus may serve as a beacon pointing toward the onset of early emphysema. Furthermore, recent findings in our laboratory have led us to believe that regional alterations in blood flow parameters may not only serve as an early marker for inflammatory processes but may also be a major etiologic component of the pathologic process, leading to emphysema in a subset of the smoking population (not all smokers have emphysema). We present preliminary evidence that leads us to a new hypothesis relating emphysema to an inherent loss of the ability to blunt regional hypoxic pulmonary vasoconstriction (HPV) when the regional hypoxia is derived from inflammatory events.

MDCT provides the ability to image the lung with a theoretical *in vivo* resolution of approximately 0.5 mm. The whole lung can be imaged at this resolution in approximately 10 seconds, which is well within a single breath-hold. Scanner rotation speeds are on the order of 300 milliseconds per revolution, and recently there has been the introduction of dual-source CT (Somatom Definition; Siemens Medical Systems, Erlangen, Germany) whereby two X-ray guns are placed on the gantry, serving to double the temporal resolution of the scanner system, and thus opening up the possibility of dual energy scanning, which allows for sensitive discrimination between tissue types and contrast agents, such as iodine and xenon. Dynamic imaging via CT allows for regional quantitative assessment of parenchymal perfusion and ventilation. With advances in image-processing methods, the lung, lobes, bronchial tree, and vascular trees can be extracted and quantitatively assessed. Density and texture measures of the lung parenchyma via MDCT imaging are now providing tools for establishing regional presence and distribution of lung pathology, which, when coupled with regional measures of function, may serve as important phenotypes within a population, serving as the starting point for the quest to define associated genotypes.

From the unique opportunity to link structure and function via MDCT, we have found evidence that, on a very regional basis, the lung is able to shut off or blunt HPV in the presence of local inflammation. This article puts forth the following series of interrelated hypotheses as follows:

- Smoking is associated with regional microinflammatory events, which in turn cause regional hypoxia.
- Smokers without the ability to shut off regional HPV in the presence of inflammation are susceptible to emphysema.
- If perfusion to the inflamed hypoxic regions is important to the evolution of emphysema, then the HPV in regions of inflammation will be compounded with reduced flow to the apical lung due to gravitational effects.

Inflammatory parenchymal lung diseases are common and are significant causes of disability and premature death. These diseases

(*Received in original form March 20, 2006; accepted in final form May 30, 2006*)

Supported in part by NIH grants R01-HL-64368-01 and R01-HL-60158-04.

Correspondence and requests for reprints should be addressed to Eric A. Hoffman, Ph.D., Department of Radiology, University of Iowa, 200 Hawkins Drive, CC701 GH, Iowa City, IA 52242. E-mail: eric-hoffman@uiowa.edu

Proc Am Thorac Soc Vol 3. pp 519–534, 2006
DOI: 10.1513/pats.200603-086MS
Internet address: www.atsjournals.org

are the result of subacute/chronic or chronic inflammatory processes, and are linked to cigarette smoking, either as a cause or as a modifying agent. Current methods for the assessment of these disorders include measures of lung function, radiologic techniques such as CT scanning (1), radionuclear-based ventilation/perfusion lung scans (2–5), use of hyperpolarized 3-He gas (2, 6–8) in conjunction with magnetic resonance imaging (MRI), or direct assessment of lung pathology. Much of the focus on mechanisms of improvement has focused on lung mechanics (9–11). Remy-Jardin and colleagues (1) have provided a unique observation via CT demonstrating that longitudinal changes leading to an emphysema-like lung begin with micronodular and ground-glass appearances in the lung field correlating to bronchiolitis and parenchymal inflammation. However, although many individuals with these regional inflammatory processes progressed toward an increased emphysema burden (in the inflamed regions), not all subjects with inflammation evolved toward emphysema, suggesting that there may be important differences in the ways individuals react to regional inflammatory processes in the lung.

Although respiratory textbooks teach that it is teleologically advantageous to shunt blood away from regions of poor ventilation, when the poor ventilation is caused by inflammatory processes (i.e., micronodules and ground glass found by Remy-Jardin and colleagues [1]), the best hope for resolution of the inflammation is to maintain an adequate blood supply to that area. In fact, three of the four components of the classic description of the inflammatory response—calor (warmth), rubor (redness), and tumor (swelling)—reflect increased local blood flow (dolor, or pain, being the fourth). Schuster and colleagues and Gust and colleagues, in two key papers using positron emission tomography (PET) imaging to study mechanisms of hypoxemia in acute lung injury (12, 13), showed that HPV is shut off when even a very small dose of endotoxin has been delivered to the lung. Recent work in our laboratory using MDCT, and outlined below, provides further evidence of local HPV inhibition in the presence of regional inflammation concomitant with other areas of the lung maintaining a healthy HPV response.

Recent conclusions from the National Emphysema Treatment Trial (NETT) (14) show that the subgroup most likely to respond to surgery with improvement in exercise and quality of life are subjects with low exercise capabilities and apical predominance of the disease (15). If a key feature of the disease is the shunting of perfusion away from inflamed regions of lung, thus reducing blood flow to regions needing perfusion to resolve the inflammation, then the normally reduced perfusion to the lung apices in upright humans likely contributes significantly to susceptibility of the parenchyma to adverse responses to inflammatory processes in the confounding presence of unconstrained HPV.

Measures based on airflow or other measures of global lung function have reached their limits in their ability to provide new insights into the etiology of the disease, or even in leading us to an understanding of how lung volume reduction, in late stages of the disease, provides patient improvements. A number of articles have been written in which attempts are made to explain improvements of physiologic status post-LVRS (9, 16) on the basis of lung mechanics, and we find it difficult to understand how these relate to the observations from the NETT (15) showing that subjects with apical but not basal prevalence of disease receive the greatest benefit from surgery. However, if regional pulmonary perfusion is again brought into consideration, it makes sense that, if one removes apical lung that is not contributing well to gas exchange and blood is shunted to less diseased basal lung, gas exchange will be improved. Furthermore, by removing a diseased portion of the basal lung when the disease is predominantly basal, then it is likely that blood will be preferentially shunted to the contralateral basal lung. Using scintigraphy to assess regional $\dot{V}/\dot{Q}$, Moonen and colleagues (2) have recently concluded that an important mechanism for improvement in functional status post-LVRS relates to the reduction of regional shunt (i.e., blood flow may be directed toward regions of improved ventilation whereas regions receiving blood flow but that have poor ventilation are removed).

A recent international consensus statement on the diagnosis and therapy of COPD—the Global Strategy for the Diagnosis, Management, and Prevention of Chronic Obstructive Lung Disease (GOLD [Global Initiative for Chronic Obstructive Lung Disease])—has established diagnostic criteria that currently do not include CT findings (17). This is not surprising given that the consensus statement has been developed in part for the World Health Organization. It is notable that the summary makes the observation that different inflammatory events occur "in various parts of the lung," a reference to the marked heterogeneity of the disease which cannot be defined without imaging. Of interest also are the future recommended research directions, which include identifying better defining characteristics of COPD, developing other measures to assess and monitor COPD, and recognizing the increasing need to identify earlier cases of the disease, all potential outcomes of improvements to quantitative lung imaging.

High-resolution volumetric MDCT with parenchymal structural analysis, bolus contrast–based measurement of pulmonary perfusion parameters, and xenon-enhanced measurement of regional ventilation can provide objective and reproducible measures to phenotypically describe the normal and the inflamed lung and can provide important information regarding regional physiologic status of the lung before and after interventional procedures such as LVRS, endobronchial valve insertions to limit gas flow to proximal lung, and grommet placements to relieve trapped gas.

PHENOTYPING EMPHYSEMA

Evaluation of Disease Progression

It has been well demonstrated that lung function declines with age (18–21) and perhaps also as a result of inflammation (22). This has confounded research related to the effects of smoking cessation on lung health. There are mixed results as to whether or not smoking cessation halts the progression of emphysematous lung disease (20, 23–27). Work by Bosse and colleagues (28) attempted to take into account the aging process and suggested that the disease process is slowed if one stops smoking. However, tests were not sensitive enough to conclude this definitively. There appear to be important sex differences in the effects of cigarette smoking and cessation (29). No reliable specific biochemical markers of disease presence or progression have been identified (30), in part perhaps because of the lack of a sensitive standard to diagnose and follow the diseases. More recently, CT parameters have been shown to be likely more sensitive to disease progression (31). Furthermore, the long time course of these diseases means that clinical trials using only whole lung function as primary outcome measures require huge numbers of subjects for extremely long periods of time.

Anatomic–Physiologic Correlates of Emphysema

The lack of a direct marker for emphysema has meant that epidemiologic studies have been limited to COPD, and these perhaps give a limited view as to the epidemiology of emphysema, a specific subset of COPD but not identified as such by spirometry. The direct effect of cigarette smoking on lung function has been widely studied, with differences in relative changes in FEV_1 and the effects of smoking noted (28, 32–35). Although some studies show an increased rate of loss of FEV_1 for current smokers, there is a less significant decrease in FEV_1 for reformed

smokers (28, 32). However, more recent studies have found similar FEV_1 declines with age in both smokers and never-smokers (34, 35). It must be emphasized that these changes are likely related to bronchial hyperreactivity (36, 37) rather than to emphysema, highlighting again the need for objective measurement tools to assess emphysema.

As indicated, chronic airflow limitation (COPD) is commonly seen in emphysema, but it is not essential. Measurements of lung physiology are not always able to distinguish the abnormalities that result from emphysema from those which result from the other causes of COPD, such as chronic bronchitis or asthma (38). The strongest positive association between an index of airflow limitation, FEV_1 (% predicted) and a pathologically derived emphysema score comes from the National Institutes of Health Intermittent Positive-pressure Breathing Trial (39). There were only 48 subjects in this study, as autopsies were required for the pathologic assessment to be performed. Pulmonary function tests were performed every 3 months during the study, and were therefore available at some point before death. However, these subjects were highly selected; to enter the study, they were required to have very significant airflow obstruction, and could not be severely hypoxic; and to complete the study, they had to die during the observation period. In contrast, a study examining pathologic lung specimens taken during surgery, and appropriately fixed, showed no relationship between the pathologic emphysema rating and indices of airflow (40). Furthermore, an autopsy study enrolling 242 subjects over 6 years demonstrated that, although those subjects with greater pulmonary disability tended to have a greater degree of pathologic emphysema, 17 subjects with greater than 30% pathologic emphysema had no evidence for clinical COPD (41). Other pulmonary function tests—namely, diffusing capacity for carbon monoxide (D_{LCO}) and the exponential description of the deflation pressure/volume curve (K)—have been used to identify, and to obtain a measure of, severity for pulmonary emphysema. A number of studies have found that measurement of D_{LCO} has a very weak correlation with the pathologic assessment of emphysema (42–44). Measurements of elastic recoil pressure curves in life compared with pathologic assessment of emphysema at subsequent lung resection or postmortem have yielded conflicting results on the value of static compliance and K as a measure of emphysema (45–49). More recent studies show a weak but significant correlation between K and macroscopic emphysema ($r = 0.49$) (47, 48), with K believed to be a measure of alveolar distensibility. This background highlights the continuing search for a marker for emphysema presence and severity.

Vascular and Intravascular Alterations in Early Stages of Parenchymal Lung Disease

Increased margination of the neutrophils in the small blood vessels in the lung has been demonstrated in smokers (50–55). One of the earliest abnormalities may therefore be regional change in perfusion of affected lung regions. As the emphysematous lesions develop in the peripheral lung, there is not only destruction of the terminal air units but also gross destruction of the microvasculature of the lung (55–57). These changes, in the vascular bed and alveolar wall, may occur at the same time; however, it is probable that the changes in vascular perfusion occur slightly earlier than the alveolar wall changes, in keeping with a primary role played by the blood neutrophils. In an elastase-induced emphysema pig model, it has been shown that vascular perfusion is reduced in early emphysematous lesions using single photon emission computed tomography (SPECT) scanning (58). In this model in which the elastase is injected into the lung, there are initially areas of increased lung density, the result of edema and alveolar hemorrhage. In a guinea pig model of emphysema, muscularization of the pulmonary arterioles occurs well before any evidence of emphysema, suggesting another potential mechanism for alterations in blood flow as an early feature in emphysema development (59). Hyde and colleagues (60) have recently demonstrated that, in the adult rabbit, blood flow is significantly diverted from inflamed lung. The presence and magnitude of both pulmonary and bronchial blood flow have been shown to effect the recovery of the lung from bronchoconstriction and the clearance of aerosol or noxious particles (61–64). Thus, although there is the notion that blood flow alterations serve as a tag of inflammation, the physiology remains largely unknown, and its elucidation in the *in vivo* system will provide important new information as well as a tool for further investigations. As we suggest in the first part of this article, pulmonary perfusion abnormalities may be a primary cause of emphysema, rather than a secondary phenomenon.

THE SCANNERS

X-Ray CT

Volumetric physiologic imaging had its beginning in the mid-1970s with the Dynamic Spatial Reconstructor (DSR), which supported 14 X-ray guns on a continuous rotating gantry and was purpose-built to provide dynamic volumetric images of the heart and lungs (65). Much of the work establishing the accuracy and precision of volumetric lung imaging was performed on the DSR (65, 66). Commercial imaging technology lagged significantly behind this early work. The electron beam CT (EBCT) (67) emerged in the early to mid-1980s as another purpose-built scanner that entered the commercial arena. EBCT had no moving parts and swept an electron beam along parallel X-ray targets to achieve improved scan speeds of up to 50 milliseconds per slice pair and eight stacked slices in approximately 224 milliseconds. There have been rapid advances in speed and resolution with the advent of MDCT (68). Its cone-beam spiral CT uses a two-dimensional (2D) detector array, allowing larger scanning range in shorter time with higher image resolution (69, 70). The ability to acquire multiple image slices per rotation with rotation speeds as short as 0.33 seconds allows for a significant reduction in acquisition time. Faster scan times will significantly impact functional imaging protocols where the rate of perfusion of a contrast agent is measured over time or where gated imaging is needed. We believe the future of lung assessment resides with true dynamic low-dose volumetric CT scanners that image at least one-third of the thorax with 0.5-mm isotropic voxels and a full rotation scan aperture of 150 milliseconds and that have superior contrast resolution for radiopaque gas and injected contrast detection. The system will be likely coupled with a low-Tesla MR scanner that will be used to complement the information available from the CT image. Patients will be scanned frequently by low-Tesla MR and less frequently over time by use of the CT component. To this end, MDCT has evolved to where typical scanners now acquire 64 slices in a single rotation spanning up to 4 cm of the z-axis of the chest, and manufacturers have shown prototypes supporting up to 256-slice scanning (Toshiba, Tochigi, Japan) in a single rotation. A dual X-ray source scanner (Definition; Siemens, Erlangen, Germany) provides significant increases in speed and opens the possibility of dual energy scanning. With dual energy scanning (setting the two X-ray sources at different kV, such as 80 and 140 kV), there is a density shift in regions with interposed contrast agents, such as inhaled xenon gas or injected iodinated contrast agents, without a concomitant shift in normal body tissues. As such, one can subtract away the tissues from the images derived from the two imaging chains while leaving behind the xenon or iodine signal as an index of regional lung function.

Customized compounds (71) can now be designed to selectively target tissues based on particular characteristics of the tissue.

MRI

Over the past 10 years, there has been renewed interest in applying MRI to the lung. Of particular interest has been the use of hyperpolarized helium (HP 3-He) MRI. Methods include the following: measures of peripheral airspace size (72–75), visualization of ventilation distribution at high spatial resolution (76–79), and assessment of gas flow patterns within the lobar and segmental airways (80–82). Furthermore, the speed of depolarization of HP 3-He enables direct measurement of regional partial pressure of oxygen and thus allows for an inference of regional gas exchange (83–85). Critical to HP 3-He, and its more recent counterpart, HP Xe, is the need to quantitate the resultant images. We believe that MDCT may serve as a gold standard against which these quantitative measures can be developed.

SCANNING PROTOCOLS

Within the APPENDIX, we provide the scanning protocols associated with our anatomic and functional imaging studies. These protocols include the radiation estimations. Radiation dose remains the limiting factor in determining the benefit of the technology relative to the risk when applied to a particular study. Hoffman and coworkers have discussed radiation dose considerations more fully elsewhere (86).

QUANTITATIVE IMAGE ANALYSIS

Critical to taking full advantage of MDCT (and MRI) is the ability to objectively evaluate the information content of the images. In the case of the lung, the starting point is reliable detection of the lungs, lobes, airways, and blood vessels, followed by an analysis of parenchymal density and texture, and finally a regional quantification of regional ventilation and perfusion parameters.

Over the past 25 to 30 years, quantitative imaging has been the focus in our laboratory to study the lung, and has included biplane fluoroscopy methods for estimating lung stress–strain (pleural pressure) (87, 88) and X-ray CT methods for the purpose of evaluating the normal physiology of the lung. CT has been validated as a tool for assessing lung volume (89), regional air content (90, 91), regional lung expansion (91–93), airway segmentation (93–95), and vessel segmentation (96, 97). These studies were focused on the use of purpose-built scanner systems (the DSR [98]) and the electron beam CT scanner (67). More recently, with the emergence of MDCT scanners, a Bioengineering Research Partnership Grant from the NIH (HL-064368, E.A.H. and G.M.) has served to bring together investigators from multiple institutions from around the world to establish MDCT as a comprehensive imaging modality to assess both structure and function of the human lung, to establish the normal range of airway and vascular structure, parenchymal density, and texture together with regional characteristics of ventilation and perfusion. Perfusion is assessed via dynamic imaging of first-pass kinetics of a bolus injection of iodinated contrast agent and ventilation via the wash-in and washout characteristics of stable, radio-dense xenon gas. A cohort of normal human subjects are being imaged over 4 decades of age range, both male and female, across a broad spectrum of racial and ethnic backgrounds to establish an atlas of the normal lung, against which an unknown lung can be statistically compared for abnormality.

Respiratory Gating

To detect early pathology and small, incremental progression of disease, one must take great care to appropriately calibrate the scanner on a regular basis, taking into account the imaging characteristics of the scanner and image reconstruction algorithms. Perhaps even more important, however, is to also take great care that the lung is imaged at standardized volumes, just as one coaches a patient in the pulmonary function laboratory. To this end, we have established a respiratory gating methodology that allows us to accurately gate image acquisition to lung volume in human subjects, using either a pneumotachograph, an inductance plethysmograph (Respitrace; Research Instrumentation Associates, Inc., Chesterland, OH), or turbine flowmeter signal. With modified scanner software, one is able to reduce the scanner pitch (table increment per 360° gantry rotation divided by beam collimation) down to 0.1 for retrospective respiratory-gated spiral imaging. Within our laboratory, we have built a fully integrated software/hardware solution using the pneumotachometer and inductance plethysmograph and are currently building a second system based on the turbine for Xe imaging in humans. We use software written in LabView (National Instruments, Austin, TX) to record patient physiology (including airway pressure, ECG, blood pressures, etc.) and then we are able to gate the scanner on and off according to the physiologic parameters of interest. Scanner manufacturers are currently providing simple pneumatic belts for respiratory gating. Little work has currently been done to verify the accuracy of these belts under various conditions, such as shifts from abdominal to ribcage breathing and prone versus supine scanning.

The segmentation of the lung, lobes, airway, and pulmonary vascular bed is described together with methods for assessing lung texture (parenchymal pathologies), perfusion, and ventilation in the following sections.

Lung Segmentation

Automated segmentation of the lungs from a 3D set of CT images is a crucial first step in the quantitative analysis of pulmonary physiology or pathophysiology. With large 3D image volumes becoming commonplace, routine manual segmentation to identify regions of interest (ROIs) is too cumbersome and time-consuming. In addition, manual analysis has significant interobserver and intraobserver variability.

We have developed and validated a segmentation method to accurately extract the lungs from CT images (99) (Figure 1). This approach, which can be used automatically or semiautomatically, relies on thresholding to obtain approximate initial lung masks. These lung masks are refined using topologic analysis (e.g., to delete cavities and small disconnected pieces) and specialized processing to enforce anatomic constraints (e.g., using a graph search to find the most likely location of the line separating the left and right lung). Experimental studies using images acquired from humans have shown our method to be very accurate: computer-generated and manually defined lung areas (in pixels) correlated very well in individual slices ($r = 0.99$).

Lobe Segmentation

Zhang and colleagues (100) have developed a semiautomatic method for identifying the fissures in CT images (Figure 1). This method uses a combination of anatomic features and CT image features to identify the fissures on 2D transverse slices. These features are combined into a cost function that reflects the likelihood that a pixel lays on the fissure. A graph search, which is a heuristic cost-based search technique, is used to find a path between the endpoints. Graph searching finds the minimum cost path between the two endpoints, where the cost function definition reflects the problem of interest. The user must initialize the process once for each fissure of interest, but once the procedure has been initialized, the entire 3D surface can be automatically identified. The overall root mean square error between manual

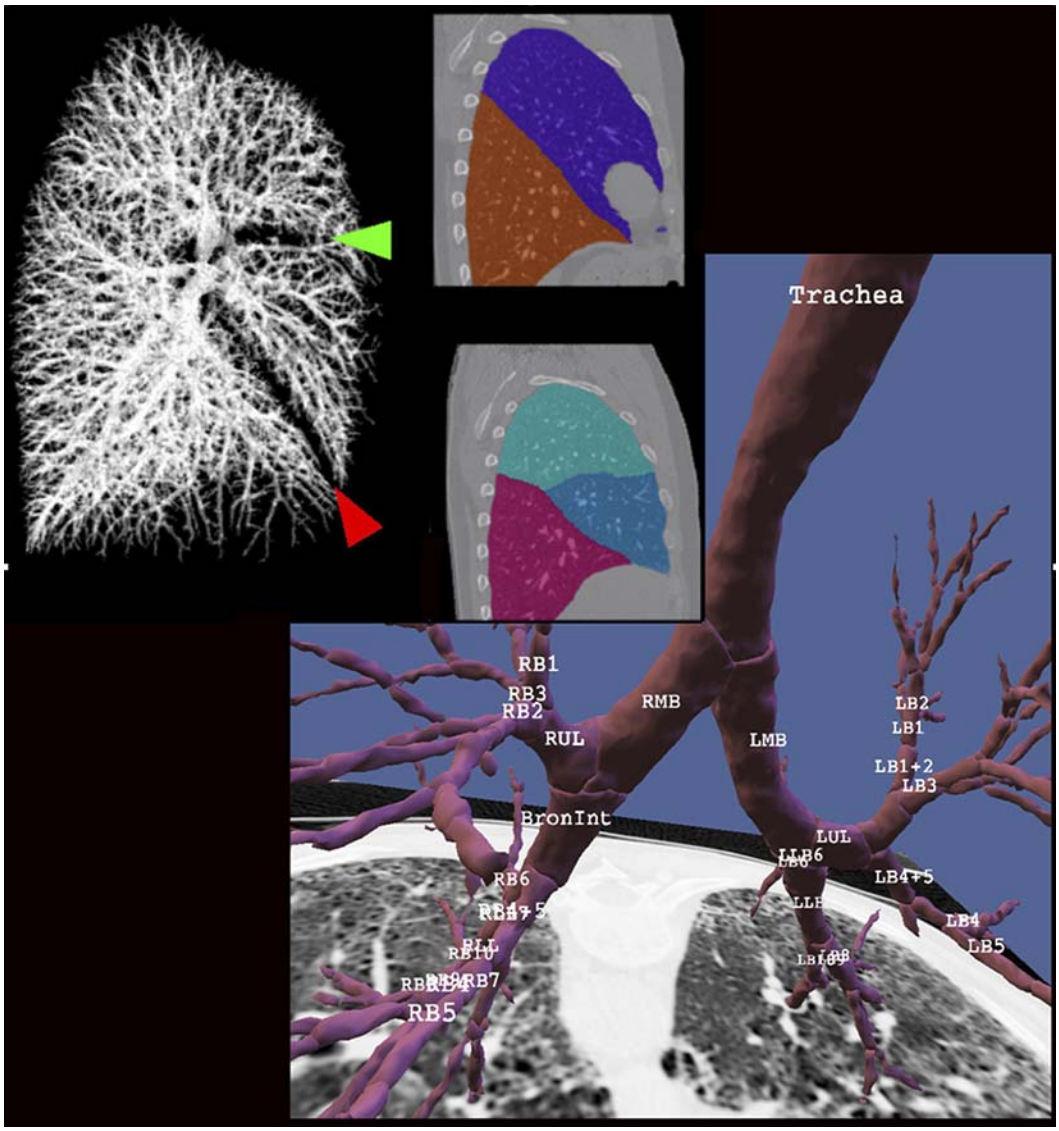

Figure 1. Results of vascular (*upper left*), lobe (*middle*), and airway (*lower right*) segmentation. After the airways are identified (segmented) and the centerline and branchpoints are identified, then the airway tree is automatically labeled. The lobar fissures are identified by the geometry of the segmented blood vessels as shown by the *red* and *green arrowheads* shown in the *upper left panel*. *L* = left, *R* = right, *B* = broncus, *UL* = upper lobe, *M* = middle lobe, *LL* = lower lobe.

tracing of the fissure and our semiautomatic method is about 2 pixels. Under development are methods to automatically initiate the lobe segmentation process through the development of a standard lung atlas representing the average shape of the normal human lung. The individual is then matched to the atlas and the location of the fissures in the atlas serve as the initial guess for the search initiation. More recent work from the laboratory has used an anatomic pulmonary atlas with *a priori* knowledge about lobar fissure shapes from a set of presegmented training datasets to achieve a fully automatic lobe segmentation (101).

Airway Lumen and Wall Segmentation

Airways of interest range in size from 1- to 15-mm inside diameter, and the software determines the borders of the inner and outer airway walls (102). The small airways have very thin walls, typically on the order of 10 to 15% of the inner diameter. The established full-width at half-maximum method for measurement can give very inaccurate results for these small thin-walled structures. To address this problem, we use a new method of estimating the airway wall locations. We first assess the point spread function of the particular scanner/slice selection/reconstruction algorithm of interest and then use a model-based deconvolution to account for blur introduced in the scanning process. This approach was shown to be more accurate than previously used wall detection methods, especially for thin-walled structures. Phantom studies have demonstrated the new method to be applicable across a wide variety of airway sizes (102, 103). As shown in Figure 2, once the airway tree has been identified in 3D, airway paths can be "straightened" into a pathway "pipe" view to allow for assessment of the local geometry perpendicular to the airway centerline.

To identify the airway tree structure, Tschirren and colleagues (104, 105) have developed an automated segmentation, skeletonization, and branchpoint matching method. The airway tree is identified using a seeded region growing algorithm, starting from an automatically identified seed point within the trachea. The algorithm is designed so that it can overcome subtle gray-level changes (e.g., those caused by beam hardening). On the other hand, a "leaking" into the surrounding lung tissue can be avoided. The implementation of the algorithm uses graph algorithms that make it fast and memory friendly. The method reliably segments the first five to six airway generations. The binary airway tree is then skeletonized to identify the 3D centerlines

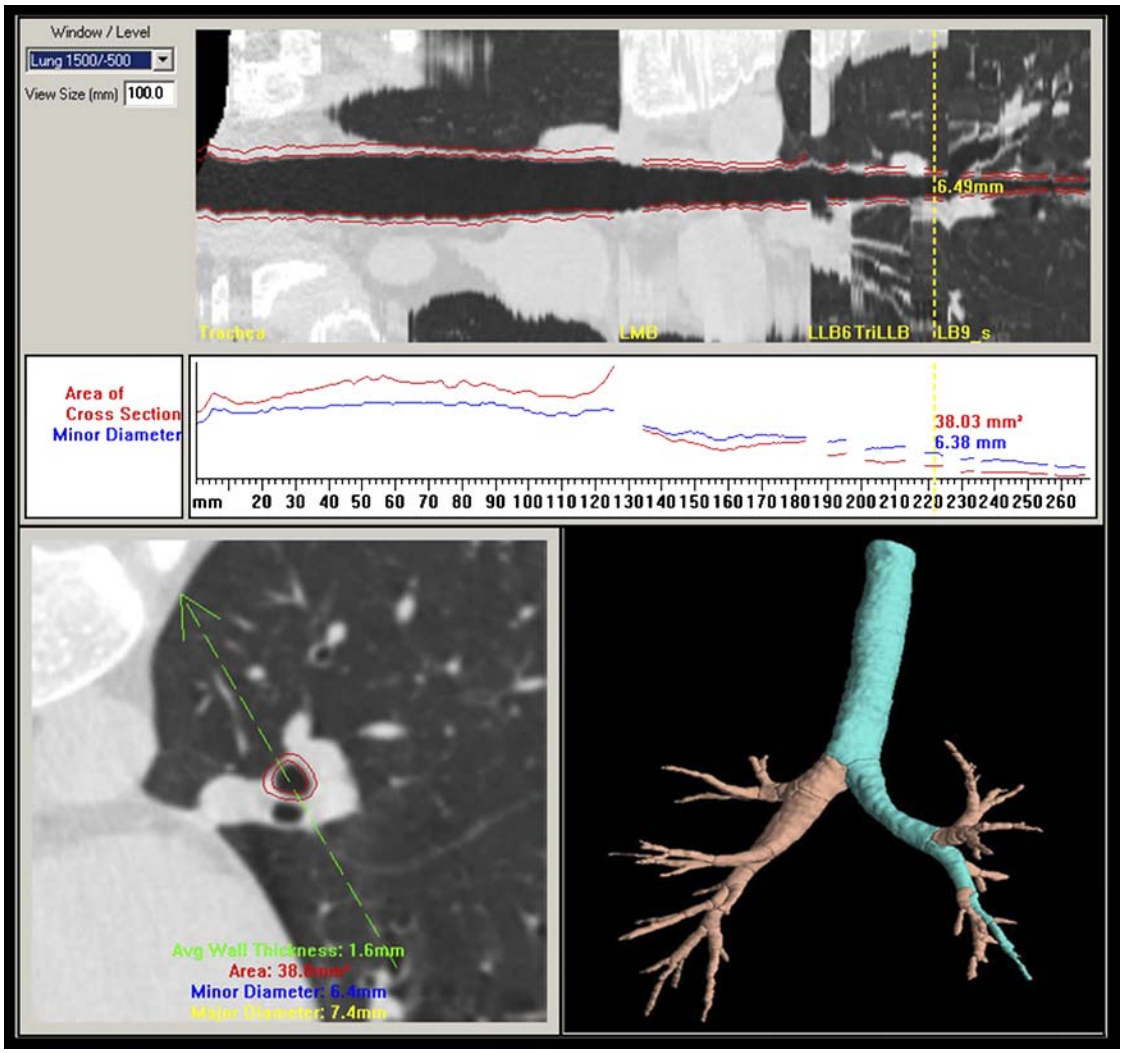

Figure 2. Once the three-dimensional airway tree has been identified and labeled, paths can be identified and straightened so as to provide luminal and wall dimensions measured as a function of the distance along the path and perpendicular to the local long axis. The airway cross-section corresponding to the *yellow vertical line* in the *upper panel* is shown in the *lower left panel*. The *green arrow* in the *lower left panel* can be rotated about the centerline of the airway to alter the cut plane shown in the straightened airway presented in the *upper panel*.

of individual branches and to determine the branchpoint locations. A sequential 3D thinning algorithm reported by Palagyi and colleagues (106) was customized for our application. False branches are pruned, and the resulting skeleton is guaranteed to lie in the middle of the cylindrically shaped airway segments. Branchpoints are used to define airway tree segments, which are then automatically labeled with a modified standardized nomenclature that we have established that takes into account the most common variability between individuals. This nomenclature (shown in Figure 1) can be applied to images of multiple lung volumes of the same individual to allow us to track the change in airway dimensions along an airway path as well as the change in airway dimensions with change in lung volume. Our airway segmentation methods have been shown to be robust in the presence of significant emphysema and when applied to images acquired using low-dose scanning protocols. In Figure 3, we demonstrate the ability to extract an airway tree of a subject with interstitial lung disease in which there is considerable mixed pathology, including emphysema, honeycombing, traction bronchiectasis, and fibrosis.

Parenchymal Analysis

Computer-based methods for objective quantitation of MDCT datasets to compare normal and diseased lung parenchyma are increasingly being used in conjunction with 2D datasets. A cornerstone of lung assessment for emphysema by MDCT scanning has become known as the density mask. The basis of the density mask is that a CT scanner, if properly calibrated, reconstructs air with a Hounsfield unit (HU = standardized unit of X-ray attenuation) of −1,000, water as 0, and blood/tissue as approximately +55. Because the lung is composed of only air or blood/tissue densities and because the HU is linear between these two values, one is able to assess the percentage of air and percentage of blood/tissue in each reconstructed voxel. Because emphysema is defined as an enlargement of the peripheral airspaces associated with parenchymal destruction, the HU of a voxel becomes an index of presence and severity of the disease. By empirically defining a given lung density at full inspiration as emphysema, one can set a density threshold (HU) below which all voxels are considered to be emphysema (107–114). This is the so-called density mask. It has been observed that the density mask for severe emphysema in 5-mm-thin or thinner slices falls at approximately −950 HU, moderate emphysema at approximately −910 HU, and mild at approximately −850 HU. By identifying where the lung is in the image and then dividing the lung into left and right, apical, mid, and basal regions, and then dividing these regions into the "core" and "peel," we are able to begin to establish phenotypes for populations (distinguished, for instance, by sex, ethnicity, α_1-antitrypsin deficiency, and now possibly subpopulations of smokers), differentiating populations based on

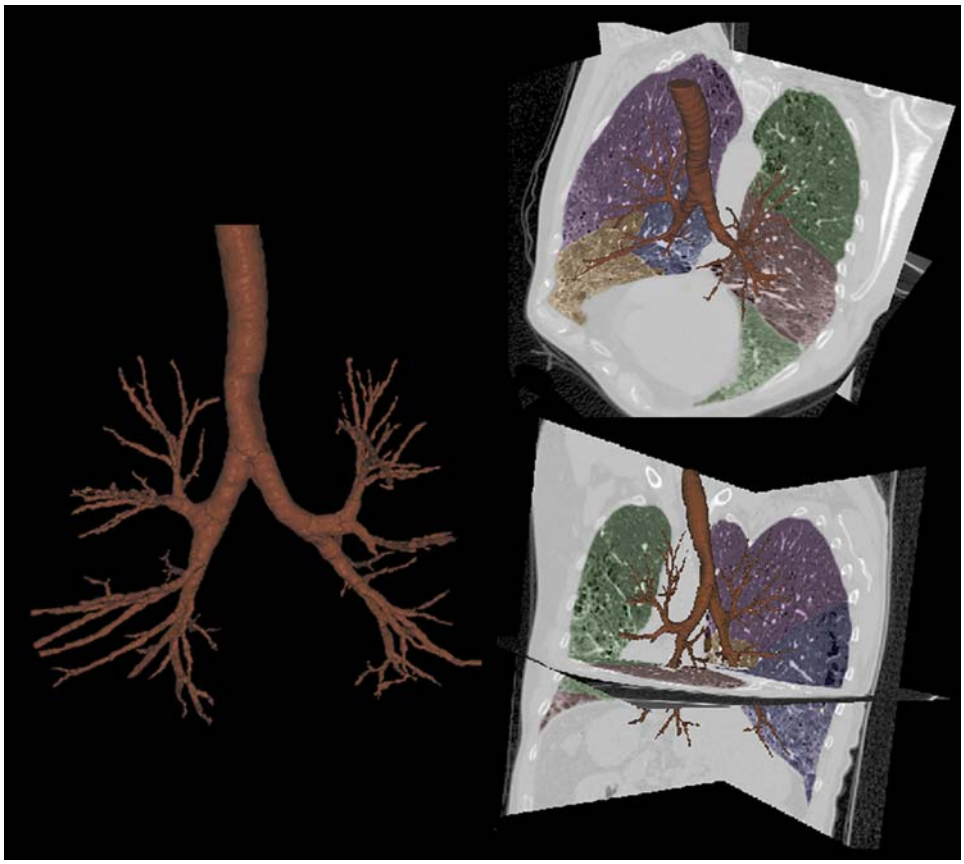

Figure 3. Demonstration of the ability to extract a detailed airway tree from computed tomography (CT) scans of a patient with significant mixed-lung pathology. The images show emphysema, honeycombing, traction bronchiectasis, and fibrosis.

characteristics of the pattern and severity of emphysema. Adams and coworkers have pointed out the importance of imaging without contrast agent when using HU as a measure of emphysema (107). A density-masking approach alone is not sufficient to accurately distinguish normal from diseased lung (115–117), especially in the case of early or mixed pathologic processes. The density mask is, however, particularly useful in characterizing mild/moderate and severe emphysema and has been used in the NETT to identify subgroups of patients who show benefit from LVRS (15). With the increased use of CT to screen for lung cancer (118) and coronary calcium (119), Reddy and colleagues have demonstrated the utility of using these same scans to characterize the presence and distribution of emphysema (120, 121). Care must be taken when one uses CT to quantitate parenchymal characteristics because scanner miscalibration and reconstruction kernels can cause some variations in the measurements (122–124). Furthermore, because the X-ray is not a single energy, beam-hardening artifacts, if not well corrected for by the manufacturers, can cause additional errors.

As our image analysis methods have evolved, we have integrated the tools into a PC-based comprehensive lung image analysis package called Pulmonary Analysis Software Suite (PASS). In addition to the traditional density mask discussed above, we have incorporated an additional measure, one proposed by Mishima and colleagues (125), which has been termed the "fractal dimensions" or "alpha." Alpha is the slope of the log–log relationship of hole size versus percentage of holes at that size. The notion is that initially a random set of holes evolves in lung regions and, as such, the log–log plot of hole size versus percentage of holes is linear. However, once the initial holes have evolved, there is a greater likelihood that these holes will have destabilized the lung mechanically and the small holes will combine to form bigger holes as opposed to more small holes appearing. Thus, the slope of the log–log plot diminishes. In this way, alpha becomes an index of disease severity.

Texture (Adaptive Multiple-Feature Method)

High-resolution CT (HRCT) enhances the resolving power of the image (126–130), allowing detection of less severe emphysema. Various computer-assisted texture-based methods have successfully been used for tissue characterization. Traditional methods of texture analysis can be grouped into statistical, structural, and hybrid methods (131). Methods for tissue classification typically rely on region gray-scale statistical measures (i.e., mean, variance, frequency histogram) or textural measures (autocorrelation, co-occurrence matrices, run-length matrices, etc.) (107–111, 132–141).

Although simple density measures are adequate for the assessment of moderate to severe emphysema, this simple measure is inadequate in assessing early pathologic changes, detecting changes where the pathology is mixed, or detecting more complex patterns such as ground glass. We have developed and patented a unique method of texture analysis of the lung for the objective assessment of pathologic processes in which simple lung density measures are inadequate for detection or differentiation of processes. Our Adaptive Multiple-Feature Method (AMFM) assesses as many as 22 independent textural features from HRCT scans to classify a tissue pattern (116, 142, 143). The AMFM is 100% reproducible and performs as well as experienced human observers who have been told the patient diagnosis. Recently, a goal of extending the AMFM feature set from 2D to 3D (144) has been motivated by the emergence of MDCT scanners with the ability to acquire volumetric image datasets

with near isotropic (near equal dimensions in all three orthogonal directions) voxels. We have used images from the normal population studied through our Bioengineering Research Partnership (BRP) grant together with heavy smokers studied at the University of Iowa in the National Lung Screening Trial. The 3D ROIs from lung regions (50 subjects total) of normal never-smokers were identified together with normal lung from normal smokers, mild emphysema from smokers with mild COPD, and moderate to severe emphysema regions from smokers with moderate to severe COPD. Lung status was defined based on American Thoracic Society GOLD criteria for characterizing COPD derived from spirometry-based FEV_1/FVC measures. Although 2D performed as well as 3D for GOLD 2 and GOLD 3 emphysema, the 3D feature set provides a highly significant improvement in differentiating normal-appearing lung sampled from nonsmokers versus GOLD class 0 smokers.

Functional Imaging

Numerous methods have been developed to assess ventilation and perfusion, or their functional outcome, gas exchange. Although clearly useful, pulmonary function tests are global measurements of airflow, lung volumes, and gas exchange from which are inferred primary structural and functional alterations. Imaging techniques such as PET (145) and the newly emerging hyperpolarized gas imaging via MRI (146–152) offer unique, complementary regional information to X-ray CT and, as they develop, are expected to offer enhancements to the knowledge base that we propose to build into the lung atlas via MDCT.

Ventilation assessed by CT. Regional ventilation is measured from time course of CT density change during a multibreath wash-in and washout of radio-dense Xe gas (153). Studies to date have demonstrated that the optimal imaging time is at end expiration when conducting airways are filled with alveolar gas (154). Average regional time constants are similar for repeat runs reducing inspired Xe gas concentrations from 55 to 30%, but the coefficient of variation at 30% Xe is significantly greater than at 40% and higher concentrations. The addition of 30% krypton gas to 30% Xe gas provides the same contrast enhancement and signal-to-noise ratio as 40% Xe (155). Krypton has none of the unwanted side effects of higher concentrations of Xe gas. Of particular note is the observation that wash-in and washout time constants are not equal, as previously assumed. Washout is longer, specifically at higher Xe concentrations and in dependent basal lung regions (154).

Perfusion assessed by CT. Dynamic imaging methods have been used to estimate arterial, venous, and capillary transit times and capillary flow distributions (156–163). These methods involve two types of image data collection regimes: inlet–outlet detection is typically used for conducting vessels and whole organ analysis; the other data collection regime is referred to as residue detection. Residue detection is typically used alone or in conjunction with inlet detection for analysis of microvascular regions wherein the individual vessels are below the resolution of the imaging system. Various approaches for determining blood flow and/or mean transit time have been described (157, 160–170).

To assess regional parenchymal perfusion, we place a catheter in the right ventricular outflow tract in animals and in the superior vena cava in humans. A sharp (0.5 cc/kg over 2 s) bolus of iodinated contrast agent (Visipaque; GE Healthcare, Milwaukee, WI) is delivered during ECG gated axial scanning. Scanning commences one to two heartbeats before contrast injection, with lungs held at functional residual capacity. By sampling the reconstructed time-attenuation curves within the region of a pulmonary artery and the lung parenchyma, we are able to calculate regional mean transit times as well as blood flow normalized to air or tissue content (171). We are able to deconvolve the signals such that we can estimate the timing of flow within the microvascular bed (162, 172).

We have begun imaging normal human subjects to establish the image-based atlas of blood flow in the normal human lung. As part of our work to determine the differences between the normal lung and the lung of smokers, we have imaged a series of never-smokers and smokers, both falling within a GOLD category 0. As shown in Figure 4, in preliminary studies we have found that smokers, even if defined as normal by pulmonary function tests, have increased heterogeneity (coefficient of variation) of local mean transit times of the contrast agent. With voxels on the order of $0.4 \times 0.4 \times 0.4$ mm, the increased coefficient of variation shows up only when sampling of regional blood flow occurs in regions no larger than 3×3 voxels, indicating that the level of early disruption of blood flow is at the level of the microvasculature.

HPV AND ITS FAILURE IN THE PRESENCE OF INFLAMMATION

By combining the ability to assess regional lung density, ventilation, and perfusion, we now provide the initial evidence for our hypothesis introduced at the beginning of this article: in subjects with pulmonary emphysema, one major contributing factor leading to parenchymal destruction is the lack of a regional blunting of HPV when the regional hypoxia is related to regional inflammatory events (bronchiolitis or alveolar flooding).

One of the fundamental homeostatic mechanisms by which the lung preserves oxygenation in the face of injury is HPV. HPV causes pulmonary arterial blood vessels to constrict in response to local hypoxia, thus redistributing blood flow away from poorly ventilated regions and toward lung regions that are well ventilated. This response optimizes local $\dot{V}/\dot{Q}$ matching and minimizes shunt as a mechanism of hypoxemia.

Both ventilation and perfusion were measured in units of ml/min in sheep being evaluated under a protocol, approved by the University of Iowa Animal Care and Use Committee, to develop imaging methods to evaluate the functional status of the lung after placement of endobronchial valves used in humans as an alternative to LVRS.

Studies reported here were performed at the Iowa Comprehensive Lung Imaging Center using a Siemens Sensation 64 MDCT scanner, modified to allow for external scan gating to the respiratory signal, and anesthetized, supine sheep were studied. Figure 5 shows data from one sheep with the original gray-scale images shown in the *left column*, the ventilation coded image in the *middle column*, and the perfusion image shown in the *right column*. Images taken before valve placement are in the *upper row* and post–valve placement data are shown in the *lower row*. Of interest are the following: (*1*) the sheep arrived in the laboratory with pneumonia, (*2*) loss of ventilation post–valve placement is evident in the *lower middle panel*, (*3*) reflex loss of blood flow in response to the loss of ventilation due to the valve is evident in the *lower right panel*, and (*4*) perfusion shunted away from the region of the valve served to preferentially enhance perfusion in the unventilated region in the dependent lung where there was evidence of pneumonia. Other data in the laboratory have shown that when a sheep is exposed to inspired hypoxia (15% O_2), perfusion is reduced everywhere except in the region of pneumonia, and in the region of pneumonia, perfusion is enhanced.

These studies reflect earlier findings of Gust and colleagues and Schuster and colleagues (13, 173) in which endotoxin was shown to block HPV when assessing regional perfusion via use of PET. These data, coupled with the findings of perfusion

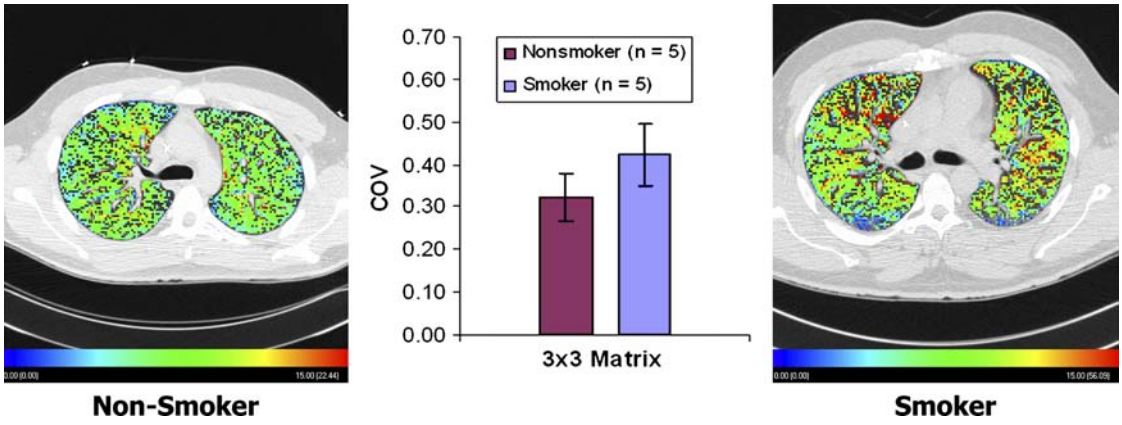

Figure 4. A normal nonsmoker and GOLD 0 smoker showing considerable increase in parenchymal perfusion heterogeneity. When sampling at increasingly coarse sample sizes, the difference in the coefficients of variation (COV) between the two groups disappears when the region-of-interest size is larger that 3 × 3 voxels (~ 1.2 mm on a side, about one-fifth to one-tenth the size of an adult ascinus) (174). Color coding ranges from 0 (*blue*) to 15 (*red*) ml/min.

disruption in smokers shown in Figure 4, indicating likely perfusion disturbance in response to inflammation, have led us to hypothesize that the normal response to hypoxia caused by inflammatory processes is to block HPV, by a process not here stipulated, so as to ensure that the cascade of events serving to fight inflammation and infection can manifest itself. We further hypothesize that, in a subset of smokers, there is an inability to block HPV in the face of inflammation and this failure sets the individual up for the evolution of the tissue destruction, which is a hallmark of emphysema. Indeed, Remy-Jardin and colleagues (1) have demonstrated,

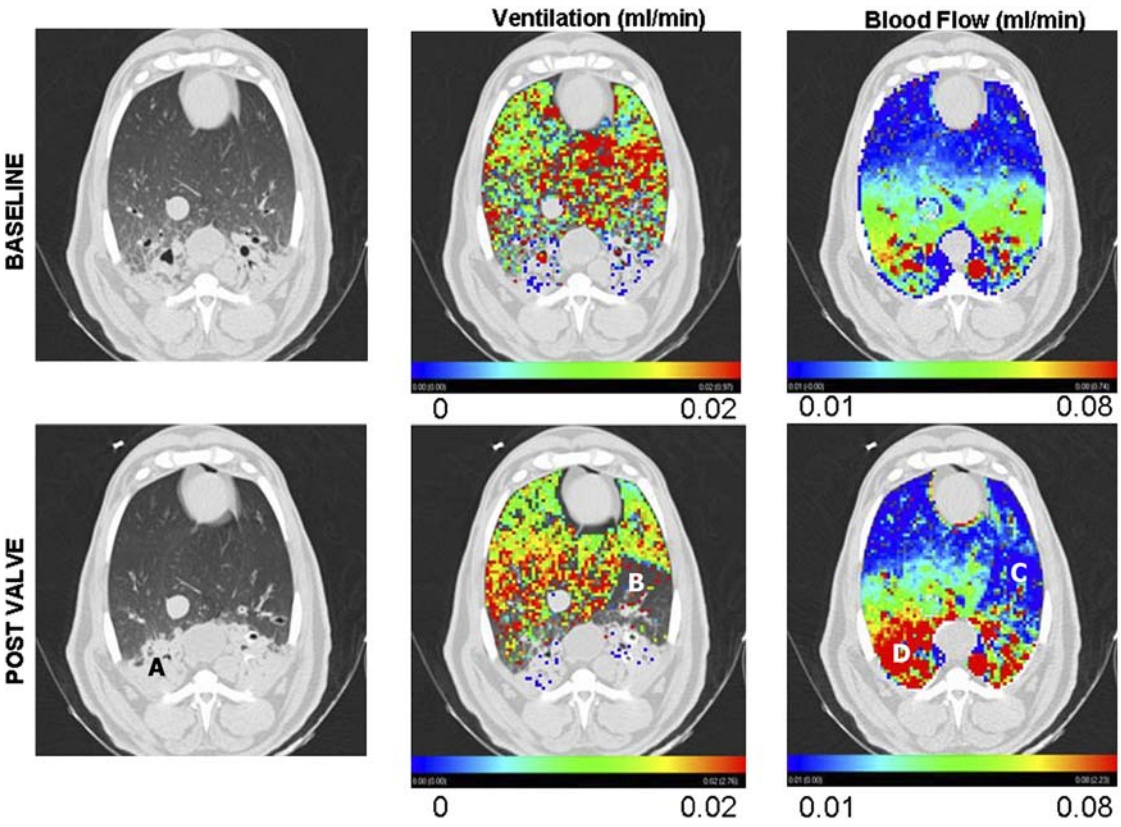

Figure 5. Before (baseline; *top row*) and after (post valve; *bottom row*) endobronchial valve placement. The *left column* provides a view of one CT section at the level of the diaphragm dome. Note the significant dependent pneumonia (*A*). The *center column* demonstrates ventilation overlayed in *color* as assessed by xenon-CT. Note that there is little ventilation in either the baseline or the post valve in the region of the dependent pneumonia. By design, there is a large region where ventilation was eliminated by the valve placement (*B*). The *right column* shows a *color overlay* of the perfusion measurements. Note that in the region (*C*) coinciding with region *B* from the central column (no ventilation due to valve placement), there is a regional loss of perfusion, indicating an intact hypoxic pulmonary vasoconstrictor (HPV) response. At the same time, in the region of pneumonia (*D*) where there is little or no ventilation, blood flow is enhanced after valve placement. Presumably, blood flow shunted away from the valve-based HPV is shunted straight toward the region of inflammation, presumably because the inflammation has served to blunt HPV in this region, leaving this region as the path of least resistance for the blood flow diverted from the region effected by HPV. Thus, this image demonstrates that lung has the ability to locally modulate HPV based on local inflammation.

as discussed earlier, in a small cohort of subjects, that, in a subset of smoker who show decline over time in pulmonary function tests, this decline is correlated with the development of emphysema in regions showing signs of ground glass and micronodules at an earlier time point. Not all smokers with ground glass and micronodules developed emphysema in these regions but these subjects also did not show a decline in pulmonary function tests.

CONCLUSIONS

We have demonstrated that MDCT provides for a comprehensive means of imaging the lung. It provides for a sensitive and objective method of assessing the lung parenchyma, airway, and functional status at the lung periphery, including measures of both ventilation and perfusion. With a combination of highly detailed anatomic information together with function measures, we are able to evaluate regional pathologic processes for the refined assessment of COPD phenotypes. We note that with the growing set of powerful tools available in the clinical setting, it becomes important to carefully establish new questions and apply appropriate imaging modalities. One must take care to apply these modalities appropriately, which brings a critical need for interdisciplinary interactions among pulmonologists, physiologists, radiologists, physicists, engineers, and many more.

Conflict of Interest Statement: E.A.H. is the founder and co-owner of VIDA Diagnostics, which is commercializing some of the software that has evolved out of his research group. He is also a member of the CT Medical Advisory Board for Siemens Medical Solutions. B.A.S. does not have a financial relationship with a commercial entity that has an interest in the subject of this manuscript. G.M. is co-owner of VIDA Diagnostics, which is commercializing some software developments coming out of his laboratory. In addition, he is a clinical investigator for Asthmatx and Emphasys.

Acknowledgment: The authors thank the entire research team of their Bioengineering Research Partnership grant whose combined efforts have made possible the findings reported within this paper. Of particular note are the contributions of Drs. Joseph Reinhardt and Milan Sonka and Juerg Tschirren, who made significant contributions to the image processing, and Drs. Deokiee Chon, Osama Saba, and David Riker, who have made significant contributions to the experimental side of the studies reported here. Abby Russi helped in the preparation of this manuscript.

References

1. Remy-Jardin M, Edme JL, Boulenguez C, Remy J, Mastora I, Sobaszek A. Longitudinal follow-up study of smoker's lung with thin-section CT in correlation with pulmonary function tests. *Radiology* 2002;222: 261–270.
2. Moonen M, Xu J, Johansson A, Thylen A, Bake B. Effects of lung volume reduction surgery on distribution of ventilation and perfusion. *Clin Physiol Funct Imaging* 2005;25:152–157.
3. Xu JH, Moonen M, Johansson A, Bake B. Distribution of ventilation-to-perfusion ratios analysed in planar scintigrams of emphysematous patients. *Clin Physiol* 2000;20:89–94.
4. Cederlund K, Hogberg S, Jorfeldt L, Larsen F, Norman M, Rasmussen E, Tylen U. Lung perfusion scintigraphy prior to lung volume reduction surgery. *Acta Radiol* 2003;44:246–251.
5. Hunsaker AR, Ingenito EP, Reilly JJ, Costello P. Lung volume reduction surgery for emphysema: correlation of CT and $\dot{V}/\dot{Q}$ imaging with physiologic mechanisms of improvement in lung function. *Radiology* 2002;222:491–498.
6. Spector ZZ, Emami K, Fischer MC, Zhu J, Ishii M, Vahdat V, Yu J, Kadlecek S, Driehuys B, Lipson DA, *et al.* Quantitative assessment of emphysema using hyperpolarized 3He magnetic resonance imaging. *Magn Reson Med* 2005;53:1341–1346.
7. Dupuich D, Berthezene Y, Clouet PL, Stupar V, Canet E, Cremillieux Y. Dynamic 3He imaging for quantification of regional lung ventilation parameters. *Magn Reson Med* 2003;50:777–783.
8. van Beek E, Wild J, Schreiber W, Kauczor H, Mugler JP III, de Lange EE. Functional MRI of the lungs using hyperpolarized 3-helium gas. *J Magn Reson Imaging* 2004;20:540–554.
9. Fessler HE, Scharf SM, Permutt S. Improvement in spirometry following lung volume reduction surgery: application of a physiologic model. *Am J Respir Crit Care Med* 2002;165:34–40.
10. Criner G, Cordova FC, Leyenson V, Roy B, Travaline J, Sudarshan S, O'Brien G, Kuzma AM, Furukawa S. Effect of lung volume reduction surgery on diaphragm strength. *Am J Respir Crit Care Med* 1998;157: 1578–1585.
11. Lewis TA, Tzeng YS, McKinstry EL, Tooker AC, Hong K, Sun Y, Mansour J, Handler Z, Albert MS. Quantification of airway diameters and 3D airway tree rendering from dynamic hyperpolarized 3He magnetic resonance imaging. *Magn Reson Med* 2005;53:474–478.
12. Schuster DP, Marklin GF. Effect of changes in inflation and blood volume on regional lung density: a PET study: 2. *J Comput Assist Tomogr* 1986;10:730–735.
13. Gust R, Kozlowski J, Stephenson AH, Schuster DP. Synergistic hemodynamic effects of low-dose endotoxin and acute lung injury. *Am J Respir Crit Care Med* 1998;157:1919–1926.
14. National Emphysema Treatment Trial Research Group. Rationale and design of the National Emphysema Treatment Trial (NETT): a prospective randomized trial of lung volume reduction surgery. *J Thorac Cardiovasc Surg* 1999;118:518–528.
15. Fishman A, Martinez F, Naunheim K, Piantadosi S, Wise R, Ries A, Weinmann G, Wood DE; National Emphysema Treatment Trial Research Group. A randomized trial comparing lung-volume-reduction surgery with medical therapy for severe emphysema. *N Engl J Med* 2003;348:2059–2073.
16. Fessler HE, Permutt S. Lung volume reduction surgery and airflow limitation. *Am J Respir Crit Care Med* 1998;157:715–722.
17. Pauwels RA, Buist AS, Calverley PM, Jenkins CR, Hurd SS. Global strategy for the diagnosis, management, and prevention of chronic obstructive pulmonary disease. NHLBI/WHO Global Initiative for Chronic Obstructive Lung Disease (GOLD) workshop summary. *Am J Respir Crit Care Med* 2001;163:1256–1276.
18. Knudson RJ, Clark DF, Kennedy TC, Knudson DE. Effect of aging alone on mechanical properties of the normal adult lung. *J Appl Physiol* 1977;43:1054–1062.
19. Muieson G, Sorbini CA, Grassi V. Respiratory function in the aged. *Bull Physiopathol Respir (Nancy)* 1971;7:973–1009.
20. Fletcher C, Petro R. The natural history of chronic airflow obstruction. *Br Med J* 1977;1:1645–1648.
21. Bosse R, Sparrow D, Garvey AJ, Costa PT, Weiss ST, Rowe JW. Cigarette smoking, aging, and decline in pulmonary function: a longitudinal study. *Arch Environ Health* 1980;35:247–252.
22. Meyer KC, Ershler W, Rosenthal NS, Lu XG, Peterson K. Immune dysregulation in the aging human lung. *Am J Respir Crit Care Med* 1996;153:1072–1079.
23. Buist AS, Nagy JM, Sexton GJ. Effect of smoking cessation on pulmonary function: a 30-month follow-up to two smoking cessation clinics. *Am Rev Respir Dis* 1979;120:953–957.
24. McCarthy DS, Craig DB, Cherniack RM. The effect of modification of smoking habit on lung function. *Am Rev Respir Dis* 1976;114:103–113.
25. Comstock GW, Brownlow WJ, Stone RW, Sartwell PE. Cigarette smoking and changes in respiratory findings. *Arch Environ Health* 1970;21: 50–57.
26. Bake B, Oxhoj H, Sixt R, Wilhelmsen L. Ventilatory lung function following two years of tobacco abstinence. *Scand J Respir Dis* 1977; 58:311–328.
27. Wilhelmsen L, Orha I, Tibblin G. Decrease in ventilatory capacity between ages of 50 and 54 in representative sample of Swedish men. *BMJ* 1969;3:553–556.
28. Bosse R, Sparrow D, Rose CL, Weiss ST. Longitudinal effect of age and smoking cessation on pulmonary function. *Am Rev Respir Dis* 1981;123:378–381.
29. Xu X, Weiss ST, Rijcken B, Schouten JP. Smoking, changes in smoking habits, and rate of decline in FEV1: new insight into gender differences. *Eur Respir J* 1994;7:1056–1061.
30. Dillon TJ, Walsh RL, Scicchitano R, Eckert B, Cleary EG, McLennan G. Plasma elastin-derived peptide levels in normal adults, children, and emphysematous subjects. Physiologic and computed tomographic scan correlates. *Am Rev Respir Dis* 1992;146:1143–1148.
31. Dirksen A, Dijkman JH, Madsen F, Stoel B, Hutchison DC, Ulrik CS, Skovgaard LT, Kok-Jensen A, Rudolphus A, Seersholm N, *et al.* A randomized clinical trial of $\alpha(1)$-antitrypsin augmentation therapy. *Am J Respir Crit Care Med* 1999;160:1468–1472.
32. Beaty TH, Menkes HA, Cohen BH, Newill CA. Risk factors associated with longitudinal change in pulmonary function. *Am Rev Respir Dis* 1984;129:660–667.
33. Camilli AE, Burrows B, Knudson RJ, Lyle SK, Lebowitz MD. Longitudinal changes in forced expiratory volume in one second in adults: effects

of smoking and smoking cessation. *Am Rev Respir Dis* 1987; 135:794–799.
34. Tager IB, Segal MR, Speizer FE, Weiss ST. The natural history of forced expiratory volumes. *Am Rev Respir Dis* 1988;138:837–849.
35. Knudson RJ, Knudson DE, Kattenborn WT, Bloom JW. Subclinical effects of cigarette smoking: a five year follow up of physiological comparisons of healthy middle aged smokers and non-smokers. *Chest* 1989;95:512–518.
36. Sherman CB. The health consequences of cigarette smoking: pulmonary diseases. *Med Clin North Am* 1992;76:355–375.
37. Vollmer WM, Johnson LR, Buist AS. Relationship of response to a bronchodilator and decline in forced expiratory volume in one second in population studies. *Am Rev Respir Dis* 1985;132:1186–1193.
38. Macklem PT. The pathophysiology of chronic bronchitis and emphysema. *Med Clin North Am* 1973;57:669–679.
39. Campbell DA, McLennan G, Coates JR, Frith PA, Gluyas PA, Latimer KM, Luke CG, Martin AJ, Roder DM, Ruffin RE, *et al.* A comparison of asthma deaths and near-fatal asthma attacks in South Australia. *Eur Respir J* 1994;7:490–497.
40. Martin AJ, Campbell DA, Gluyas PA, Coates JR, Ruffin RE, Roder DM, Latimer KM, Luke CG, Frith PA, Yellowlees PM, *et al.* Characteristics of near-fatal asthma in childhood. *Pediatr Pulmonol* 1995;20: 1–8.
41. Campbell DA, Yellowlees PM, McLennan G, Coates JR, Frith PA, Gluyas PA, Latimer KM, Luke CG, Martin AJ, Ruffin RE. Psychiatric and medical features of near fatal asthma. *Thorax* 1995;50:254–259.
42. West WW, Nagai A, Hodgkin JE, Thurlbeck WM. The National Institutes of Health Intermittent Positive Pressure Breathing trial: pathology studies. III. The diagnosis of emphysema. *Am Rev Respir Dis* 1987;135:123–129.
43. Morrison NJ, Abboud RJ, Ramadan F, Miller RR, Gibson NN, Evans KG, Nelems B, Muller NL. Comparison of single breath carbon monoxide diffusing and pressure-volume curves in detecting emphysema. *Am Rev Respir Dis* 1989;139:1179–1187.
44. Klein JS, Gamsu G, Webb WR, Golden J, Muller NL. High-resolution CT diagnosis of emphysema in symptomatic patients with normal chest radiographs and isolated low diffusing capacity. *Radiology* 1992; 182:817–821.
45. Boushy SF, Aboumrad MH, North LB, Helgason AH. Lung recoil pressure, airway resistance, and forced flows related to morphologic emphysema. *Am Rev Respir Dis* 1971;104:551–561.
46. Gelb AF, Gold WM. Wright Rr, Bruch MR, Nakel JA. Physiologic diagnosis of subclinical emphysema. *Am Rev Respir Dis* 1973;107:50–63.
47. Berend N, Skoog C, Thurlbeck WM. Pressure-volume characteristics of excised human lungs: effects of sex, age and emphysema. *J Appl Physiol* 1980;49:558–565.
48. Pare PD, Brooks LA, Bates J, Lawson LM, Nelems JM, Wright JL, Hogg JC. Exponential analysis of the lung pressure-volume curve as a predictor of pulmonary emphysema. *Am Rev Respir Dis* 1982;126: 54–61.
49. Bergin C, Muller N, Nichols DM, Lillington G, Hogg JC, Mullen B, Grymaloski MR, Osbourne S, Pare PD. The diagnosis of emphysema: a computed tomography–pathologic correlation. *Am Rev Respir Dis* 1986;133:541–546.
50. Hubbard RC, Brantly ML, Crystal RG. Proteases. In: Crystal RG, West JB, editors. The lung: scientific foundations. New York: Raven Press; 1991. pp. 1763–1773.
51. Taylor RG, Gross E, Joyce H, Holland F, Pride NB. Smoking, allergy, and the differential white blood cell count. *Thorax* 1985;40:17–22.
52. Hunninghake G, Gadek J, Kawanami O, Ferrans V, Crystal R. Inflammatory and immune processes in the human lung in health and disease: evaluation by bronchoalveolar lavage. *Am J Pathol* 1979;97:149–206.
53. Niewoehner DE. Cigarette smoking, lung inflammation, and the development of emphysema. *J Lab Clin Med* 1988;111:15–27.
54. Cohen AB, Rossi M. Neutrophils in normal lungs. *Am Rev Respir Dis* 1983;127:S3–S9.
55. Malech HL, Gallin JI. Current concepts: immunology neutrophils in human diseases. *N Engl J Med* 1987;317:687–694.
56. Janoff A. Biochemical links between cigarette smoking and emphysema. *J Appl Physiol* 1983;55:285–293.
57. Murphy KR, Marsh WR, Glezen LS, Irvin CG, Wilson MC, Larsen GL. Inflammation and the late phase reaction in asthma: the effect of polymorphonuclear leukocyte depletion on airways obstruction and bronchial hyperreactivity in an animal model. *Bull Eur Physiopathol Respir* 1986;22:48–53.
58. Noma S, Moskowitz GW, Herman PG, Khan A, Rojas KA. Pulmonary scintigraphy in elastase-induced emphysema in pigs: correlation with high-resolution computed tomography and histology. *Invest Radiol* 1992;27:429–435.
59. Wright JL, Churg A. Effect of long-term cigarette smoke exposure on pulmonary vascular structure and function in the guinea pig. *Exp Lung Res* 1991;17:997–1009.
60. Hyde DM, Downey GP, Tablin F, Rosengren S, Giclas PC, Henson PM, Worthen GS. Age-dependent neutrophil and blood flow responsiveness in acute pulmonary inflammation in rabbits. *Am J Physiol* 1997;272:L471–L478.
61. Kelly LJ, Mitzner W, Spannhake EW, Bromberger-Barnea B, Menkes HA. Pulmonary blood flow affects recovery from constriction in dog lung periphery. *J Appl Physiol* 1986;60:1554–1560.
62. Kelly L, Kolbe J, Mitzner W, Spannhake EW, Bromberger-Barnea B, Menkes H. Bronchial blood flow affects recovery from constriction in dog lung periphery. *J Appl Physiol* 1986;60:1954–1959.
63. Wagner EM, Foster WM. Importance of airway blood flow on particle clearance from the lung. *J Appl Physiol* 1996;81:1878–1883.
64. Wagner EM. Aerosol clearance by the bronchial circulation. *J Aerosol Med* 1996;9:7–10.
65. Ritman EL, Robb RA, Harris LD. Imaging physiological functions: experience with the DSR. Philadelphia: Praeger; 1985.
66. Hoffman EA, Larsen RL. Regional pulmonary blood flow via X-ray CT and biodegradable radiopaque microspheres. *Circulation* 1990;4: 111–124.
67. Boyd DP, Lipton MJ. Cardiac computed tomography. *Proc IEEE* 1983; 71:298–307.
68. Saito T, Misaki M, Shirato K, Takishima T. Three-dimensional quantitative coronary angiography. *IEEE Trans Biomed Eng* 1990;37:768–777.
69. Saito Y. Multislice X-ray CT scanner. *Med Rev* 1998;98:1–8.
70. Wang G, Lin TH, Cheng PC, Shinozaki DM. A general cone-beam reconstruction algorithm. *IEEE Trans Med Imaging* 1993;12:486–496.
71. Kao CY, Hoffman EA, Beck KC, Bellamkonda RV, Annapragada AV. Long-residence-time nano-scale liposomal iohexol for X-ray-based blood pool imaging. *Acad Radiol* 2003;10:475–483.
72. Saam BT, Yablonskiy DA, Kodibagkar VD, Leawoods JC, Gierada DS, Cooper JD, Lefrak SS, Conradi MS. MR imaging of diffusion of (3)He gas in healthy and diseased lungs. *Magn Reson Med* 2000; 44:174–179.
73. Salerno M, de Lange EE, Altes TA, Truwit JD, Brookeman JR, Mugler JP III. Emphysema: hyperpolarized helium 3 diffusion MR imaging of the lungs compared with spirometric indexes—initial experience. *Radiology* 2002;222:252–260.
74. Yablonskiy DA, Sukstanskii AL, Leawoods JC, Gierada DS, Bretthorst GL, Lefrak SS, Cooper JD, Conradi MS. Quantitative in vivo assessment of lung microstructure at the alveolar level with hyperpolarized 3He diffusion MRI. *Proc Natl Acad Sci USA* 2002;99:3111–3116.
75. Owers-Bradley JR, Fichele S, Bennattayalah A, McGloin CJ, Bowtell RW, Morgan PS, Moody AR. MR tagging of human lungs using hyperpolarized 3He gas. *J Magn Reson Imaging* 2003;17:142–146.
76. MacFall JR, Charles HC, Black RD, Middleton H, Swartz JC, Saam B, Driehuys B, Erickson C, Happer W, Cates GD, *et al.* Human lung air spaces: potential for MR imaging with hyperpolarized He-3. *Radiology* 1996;200:553–558.
77. de Lange EE, Mugler JP III, Brookeman JR, Knight-Scott J, Truwit JD, Teates CD, Daniel TM, Bogorad PL, Cates GD. Lung air spaces: MR imaging evaluation with hyperpolarized 3He gas. *Radiology* 1999;210:851–857.
78. Kauczor HU, Ebert M, Kreitner KF, Nilgens H, Surkau R, Heil W, Hofmann D, Otten EW, Thelen M. Imaging of the lungs using 3He MRI: preliminary clinical experience in 18 patients with and without lung disease. *J Magn Reson Imaging* 1997;7:538–543.
79. Altes TA, Powers PL, Knight-Scott J, Rakes G, Platts-Mills TA, de Lange EE, Alford BA, Mugler JP III, Brookeman JR. Hyperpolarized 3He MR lung ventilation imaging in asthmatics: preliminary findings. *J Magn Reson Imaging* 2001;13:378–384.
80. Viallon M, Berthezene Y, Callot V, Bourgeois M, Humblot H, Briguet A, Cremillieux Y. Dynamic imaging of hyperpolarized (3)He distribution in rat lungs using interleaved-spiral scans. *NMR Biomed* 2000; 13:207–213.
81. Salerno M, Altes TA, Brookeman JR, de Lange EE, Mugler JP III. Dynamic spiral MRI of pulmonary gas flow using hyperpolarized (3)He: preliminary studies in healthy and diseased lungs. *Magn Reson Med* 2001;46:667–677.

82. Wild JM, Paley MN, Kasuboski L, Swift A, Fichele S, Woodhouse N, Griffiths PD, van Beek EJ. Dynamic radial projection MRI of inhaled hyperpolarized 3He gas. *Magn Reson Med* 2003;49:991–997.
83. Eberle B, Weiler N, Markstaller K, Kauczor H, Deninger A, Ebert M, Grossmann T, Heil W, Lauer LO, Roberts TP, *et al.* Analysis of intrapulmonary O(2) concentration by MR imaging of inhaled hyperpolarized helium-3. *J Appl Physiol* 1999;87:2043–2052.
84. Deninger AJ, Eberle B, Ebert M, Grossmann T, Heil W, Kauczor H, Lauer L, Markstaller K, Otten E, Schmiedeskamp J, *et al.* Quantification of regional intrapulmonary oxygen partial pressure evolution during apnea by (3)He MRI. *J Magn Reson* 1999;141:207–216.
85. Rizi RR, Baumgardner JE, Ishii M, Spector ZZ, Edvinsson JM, Jalali A, Yu J, Itkin M, Lipson DA, Gefter W. Determination of regional VA/Q by hyperpolarized 3He MRI. *Magn Reson Med* 2004;52:65–72.
86. Hoffman EA, Clough AV, Christensen GE, Lin CL, McLennan G, Reinhardt JM, Simon BA, Sonka M, Tawhai MH, van Beek EJ, *et al.* The comprehensive imaging-based analysis of the lung: a forum for team science. *Acad Radiol* 2004;11:1370–1380.
87. Hoffman EA, Behrenbeck T, Chevalier PA, Wood EH. Estimation of regional pleural surface expansile forces in intact dogs. *J Appl Physiol* 1983;55:935–948.
88. Hoffman EA, Lai-Fook SJ, Wei J, Wood EH. Regional pleural surface expansile forces in intact dogs by wick catheters. *J Appl Physiol* 1983; 55:1523–1529.
89. Hoffman EA, Sinak LJ, Robb RA, Ritman EL. Noninvasive quantitative imaging of shape and volume of lungs. *J Appl Physiol* 1983;54: 1414–1421.
90. Hoffman EA. Effect of body orientation on regional lung expansion: a computed tomographic approach. *J Appl Physiol* 1985;59:468–480.
91. Hoffman EA, Ritman EL. Effect of body orientation on regional lung expansion in dog and sloth. *J Appl Physiol* 1985;59:481–491.
92. Hoffman EA, Acharya RS, Wollins JA. Computer-aided analysis of regional lung air content using three-dimensional computed tomographic images and multinomial models. *Int J Math Model* 1986;7: 1099–1116.
93. Reinhardt JM, D'Souza ND, Hoffman EA. Accurate measurement of intra-thoracic airways. *IEEE Trans Med Imaging* 1998;16:820–827.
94. Tschirren J, Hoffman EA, McLennan G, Sonka M. Intrathoracic airway trees: segmentation and airway morphology analysis from low dose CT scans. *IEEE Trans Med Imaging* 2005;24:1529–1539.
95. Tschirren J, McLennan G, Palagyi K, Hoffman E, Sonka M. Matching and anatomical labeling of human airway tree. *IEEE Trans Med Imaging* (In press)
96. Liu YH, Hoffman EA, Hagler DJ, Seward JB, Julsrud PR, Mair DD, Ritman EL. Accuracy of pulmonary vascular dimensions estimated with the dynamic spatial reconstructor. *Am J Physiol Imaging* 1986;1: 201–207.
97. Shikata H. EA H, Sonka M. Automated segmentation of pulmonary vascular tree from 3D CT images. *Prog Biomed Optics Imaging* 2004; 5:107–116.
98. Robb RA, Sinak LJ, Hoffman EA, Kinsey JH, Harris LD, Ritman EL. Dynamic volume imaging of moving organs. *J Med Syst* 1982;6:539–554.
99. Hu S, Hoffman EA, Reinhardt JM. Automatic lung segmentation for accurate quantitation of volumetric X-ray CT images. *IEEE Trans Med Imaging* 2001;20:490–498.
100. Zhang L, Hoffman EA, Reinhardt JM. Lung lobar segmentation by graph search with 3D shape constraints. In: Chen C-T, Clough AV, editors. Medical imaging 2001. Physiology and function from multidimensional images; Feb 18–20, 2001, San Diego. Bellingham, WA: SPEI. Proceedings of SPIE; vol. 4321.
101. Zhang L, Hoffman EA, Reinhardt JM. Atlas-driven lung lobe segmentation in volumetric x-ray CT images. In: Clough AV, Amini AA, editors. Medical imaging 2003. Physiology and function—methods, systems, and applications; Feb 16–18, 2003, San Diego. Bellingham, WA: SPEI. Proceedings of SPIE; vol. 5031.
102. Reinhardt JM, Raab SA, D'Souza ND, Hoffman E. Intrathoracic airway measurement: ex-vivo validation. In: Hoffman EA, editor. Medical imaging 1997. Physiology and function from multidimensional images; Feb 23–25. 1997. Newport Beach, CA. Bellingham, WA: SPEI. Proceedings of SPIE; vol. 3033.
103. Saba O, Beck K, Chon D, Nixon E, Hoffman E. Lung volume measurement reproducibility using gated-axial and spiral multi-row detector CT (MDCT) [abstract]. *Am J Respir Crit Care Med* 2003;167:A844.
104. Tschirren J, Palágyi K, Hoffman EA, Sonka M. Segmentation, skeletonization, and branchpoint matching: a fully automated quantitative evaluation of human intrathoracic airway trees. In: Dohi T, Kikinis R, editors. Proceedings of the Fifth International Conference on Medical Image Computing and Computer Assisted Intervention, 2002, Tokyo, Japan. Berlin: Springer-Verlag; 2002. pp. 12–19.
105. Tschirren J, Hoffman EA, McLennan G, Sonka M. Branchpoint labeling and matching in human airway trees. In: Clough AVA, Amir A., editors. Proceedings of the SPIE Medical Imaging, 2003, San Diego, CA; 2003. pp. 187–194.
106. Palagyi K, Tschirren J, Hoffman EA, Sonka M. Quantitative analysis of pulmonary airway tree structures. *Comput Biol Med* 2005.
107. Adams H, Bernard M, McConnochie K. An appraisal of CT pulmonary density mapping in normal subjects. *Clin Radiol* 1991;43:238–242.
108. Kinsella M, Muller NL, Abboud RT, Morrison NJ. DyBuncio A. Quantitation of emphysema by computed tomography using a "density mask" program and correlation with pulmonary function tests. *Chest* 1990;97:315–321.
109. Muller NL, Staples CA, Miller RR, Abboud RT. "Density mask": an objective method to quantitate emphysema using computed tomography. *Chest* 1988;94:782–787.
110. Gould GA, Macnee W, McLean A, Warren PM, Redpath A, Best JJK, Lamb D, Flenley DC. CT measurements of lung density in life can quantitate distal airspace enlargement: an essential defining feature of human emphysema. *Am Rev Respir Dis* 1988;137:380–392.
111. Hartley PG, Galvin JR, Hunninghake GW, Merchant JW, Yagla SJ, Speakman SB, Schwartz DA. High-resolution CT-derived measures of lung density are valid indexes of interstitial lung disease. *J Appl Physiol* 1994;76:271–277.
112. Coxson HO, Rogers RM. Quantitative computed tomography of chronic obstructive pulmonary disease. *Acad Radiol* 2005;12:1457–1463.
113. Newell JD Jr, Hogg JC, Snider GL. Report of a workshop: quantitative computed tomography scanning in longitudinal studies of emphysema. *Eur Respir J* 2004;23:769–775.
114. Stolk J, Ng WH, Bakker ME, Reiber JH, Rabe KF, Putter H, Stoel BC. Correlation between annual change in health status and computer tomography derived lung density in subjects with alpha1-antitrypsin deficiency. *Thorax* 2003;58:1027–1030.
115. Uppaluri R, Hoffman E, Schwartz D, McLennan G, Hunninghake G, Dayton C, Hartley P. Quantitative analysis of the chest CT in asbestos-exposed subjects using an adaptive multiple feature method [abstract]. *Am J Respir Crit Care Med* 1998;157:A276.
116. Uppaluri R, Mitsa T, Sonka M, Hoffman EA, McLennan G. Quantification of pulmonary emphysema from lung CT images using texture analysis. *Am J Respir Crit Care Med* 1997;156:248–254.
117. Uppaluri R, McLennan G, Enright P, Hoffman E. AMFM: a quantitative assessment of early parenchymal changes in smokers [abstract]. *Am J Respir Crit Care Med* 1998;157:A788.
118. Aberle DR, Gamsu G, Henschke CI, Naidich DP, Swensen SJ. A consensus statement of the Society of Thoracic Radiology: screening for lung cancer with helical computed tomography. *J Thorac Imaging* 2001;16:65–68.
119. Bild DE, Detrano R, Peterson D, Guerci A, Liu K, Shahar E, Ouyang P, Jackson S, Saad MF. Ethnic differences in coronary calcification: the Multi-Ethnic Study of Atherosclerosis (MESA). *Circulation* 2005; 111:1313–1320.
120. Reddy S, Berbaum K, Sprenger K, McLennan G, Hoffman E. Evaluation of emphysema-like lung parenchyma in high risk smokers: quantitation of low-dose multidetector-row computed tomography [abstract]. *Proc Am Thorac Soc* 2005;2;A259.
121. Reddy S, Barr G, Berbaum K, McLennan G, van Beek E, Hoffman E. Quantitative evaluation of emphysema: is coronary calcium screening CT a surrogate for a full lung study? Radiological Society of North America 91st Annual Meeting; Chicago, IL; 2005. p. 638.
122. Stoel BC, Bakker ME, Stolk J, Dirksen A, Stockley RA, Piitulainen E, Russi EW, Reiber JH. Comparison of the sensitivities of 5 different computed tomography scanners for the assessment of the progression of pulmonary emphysema: a phantom study. *Invest Radiol* 2004;39:1–7.
123. Shaker SB, Dirksen A, Laursen LC, Skovgaard LT, Holstein-Rathlou NH. Volume adjustment of lung density by computed tomography scans in patients with emphysema. *Acta Radiol* 2004;45:417–423.
124. Boedeker KL, McNitt-Gray MF, Rogers SR, Truong DA, Brown MS, Gjertson DW, Goldin JG. Emphysema: effect of reconstruction algorithm on CT imaging measures. *Radiology* 2004;232:295–301.
125. Mishima M, Hirai T, Itoh H, Nakano Y, Sakai H, Muro S, Nishimura K, Oku Y, Chin K, Ohi M, *et al.* Complexity of terminal airspace geometry assessed by lung computed tomography in normal subjects and patients with chronic obstructive pulmonary disease. *Proc Natl Acad Sci USA* 1999;96:8829–8834.
126. Hruban RH, Meziane MA, Zerhouni EA, Khouri NF, Fishman EK, Wheeler PS, Dumler JS, Hutchins GM. High resolution computed

tomography of inflation fixed lungs: pathologic-radiologic correlation of centrilobular emphysema. *Am Rev Respir Dis* 1987;136:935–940.
127. Miller RA, Muller NL, Vedal S, Morrison NJ, Staples CA. Limitations of computed tomography in the assessment of emphysema. *Am Rev Respir Dis* 1989;139:980–983.
128. Murata K, Itoh H, Senda M, Yonekura Y, Nishimura K, Izumi T, Oshima S, Torizuka K. Stratified impairment of pulmonary ventilation in diffuse panbronchiolitis: PET and CT studies. *J Comput Assist Tomogr* 1989;13:48–53.
129. Webb WR. High-resolution computed tomography of the lung: normal and abnormal anatomy. *Semin Roentgenol* 1991;26:110–117.
130. Sanders C. Imaging of emphysema. *Semin Respir Crit Care Med* 1992; 13:318–330.
131. Sonka M, Hlavac V, Boyle R. Image processing, analysis, and machine vision. London: Chapman and Hall; 1993.
132. Schad LR, Bluml S, Zuna I. MR tissue characterization of intracranial tumors by means of texture analysis. *Magn Reson Imaging* 1993;11: 889–896.
133. Miller P, Astley S. Classification of breast tissue by texture analysis. *Image Vis Comput* 1992;10:277–282.
134. Wu C, Chen Y. Multi-threshold dimension vector for texture analysis and its application to liver tissue classification. *Pattern Recognit* 1993; 1:137–144.
135. McPherson D, Aylward P, Knosp B, Bean J, Kerber R, Collins S, Skorton D. Ultrasound chracterization of acute myocardial ischemia by quantitative texture analysis. *Ultrason Imaging* 1986;8:227–240.
136. Skorton DJ, Collins SM, Nichols J, Pandian NG, Bean JA, Kerber RE. Quantitative texture analysis in two-dimensional echocardiography: application to the diagnosis of experimental myocardial contusion. *Circulation* 1983;68:217–223.
137. Chandrasekaran K, Aylward PE, Fleagle SR, Burns TL, Seward JB, Tajik AJ, Collins SM, Skorton DJ. Feasibility of identifying amyloid and hypertrophic cardiomyopathy with the use of computerized quantitative texture analysis of clinical echocardiographic data. *J Am Coll Cardiol* 1989;13:832–840.
138. Uppaluri R, Mitsa T, Galvin JR. Fractal analysis of high-resolution CT images as a tool for quantification of lung diseases. In: Hoffman EA, editor. Proceedings SPIE Medical Imaging: Physiology and Function from Multidimensional Images; 1995. pp. 133–142.
139. Tully RJ, Conners RW, Harlow CA, Lodwick GS. Towards computer analysis of pulmonary infiltration. *Invest Radiol* 1978;13:298–305.
140. Katsuragawa S, Kunio D, MacMahon H. Image feature analysis and computer-aided diagnosis in digital radiography: classification of normal and abnormal lungs with interstitial disease in chest images. *Med Phys* 1989;16:38–44.
141. Fleagle S, Stanford W, Burns T, Skorton D. Feasibility of quantitative texture analysis of cardiac magnetic resonance imagery: preliminary results. *SPIE Medical Imaging* 1994;2168:23–32.
142. Uppaluri R, Hoffman EA, Sonka M, Hartley P, Hunninghake GW, McLennan G. Computer recognition of regional lung disease patterns. *Am J Respir Crit Care Med* 1999;160:648–654.
143. Uppaluri R, Hoffman EA, Sonka M, Hunninghake GW, McLennan G. Interstitial lung disease: a quantitative study using the adoptive multiple feature method. *Am J Respir Crit Care Med* 1999;159:519–525.
144. Xu Y, Sonka M, McLennan G, Guo J, Hoffman E. Sensitivity and specificity of 3-D texture analysis of lung parenchymal is better than 2-D for discrimination of lung pathology in stage 0 COPD. In: Amini A, Manduca A, editors. Proceedings SPIE Medical Imaging. 2005. pp. 474–485.
145. Jones HA. Inflammation imaging. *Proc Am Thorac Soc* 2005;2:513–514.
146. Mills GH, Wild JM, Eberle B, Van Beek EJ. Functional magnetic resonance imaging of the lung. *Br J Anaesth* 2003;91:16–30.
147. Peces-Barba G, Ruiz-Cabello J, Cremillieux Y, Rodriguez I, Dupuich D, Callot V, Ortega M, Rubio Arbo ML, Cortijo M, Gonzalez-Mangado N. Helium-3 MRI diffusion coefficient: correlation to morphometry in a model of mild emphysema. *Eur Respir J* 2003;22:14–19.
148. Rizi RR, Lipson DA, Dimitrov IE, Ishii M, Roberts DA. Operating characteristics of hyperpolarized 3He and arterial spin tagging in MR imaging of ventilation and perfusion in healthy subjects. *Acad Radiol* 2003;10:502–508.
149. Kauczor HU, Hanke A, Van Beek EJ. Assessment of lung ventilation by MR imaging: current status and future perspectives. *Eur Radiol* 2002;12:1962–1970.
150. Deninger AJ, Mansson S, Petersson JS, Pettersson G, Magnusson P, Svensson J, Fridlund B, Hansson G, Erjefeldt I, Wollmer P, *et al.* Quantitative measurement of regional lung ventilation using 3He MRI. *Magn Reson Med* 2002;48:223–232.
151. Lipson DA, Roberts DA, Hansen-Flaschen J, Gentile TR, Jones G, Thompson A, Dimitrov IE, Palevsky HI, Leigh JS, Schnall M, *et al.* Pulmonary ventilation and perfusion scanning using hyperpolarized helium-3 MRI and arterial spin tagging in healthy normal subjects and in pulmonary embolism and orthotopic lung transplant patients. *Magn Reson Med* 2002;47:1073–1076.
152. Moller HE, Chen XJ, Saam B, Hagspiel KD, Johnson GA, Altes TA, de Lange EE, Kauczor HU. MRI of the lungs using hyperpolarized noble gases. *Magn Reson Med* 2002;47:1029–1051.
153. Tajik JK, Chon D, Won C, Tran BQ, Hoffman EA. Subsecond multisection CT of regional pulmonary ventilation. *Acad Radiol* 2002;9:130–146.
154. Chon D, Simon BA, Beck KC, Shikata H, Saba OI, Won C, Hoffman EA. Differences in regional wash-in and wash-out time constants for xenon-CT ventilation studies. *Respir Physiol Neurobiol* 2005;148:65–83.
155. Chon D, Beck K, Shikata H, Saba O, Simon B, Hoffman E. Effect of reduce inhaled [xenon] and [krypton] supplementation of signal noise of regional CT-based ventilation measurements [abstract]. *Am J Respir Crit Care Med* 2004;167:A547.
156. Ayappa I, Brown LV, Wang PM, Lai-Fook SJ. Arterial, capillary, and venous transit times and dispersion measured in isolated rabbit lungs. *J Appl Physiol* 1995;79:261–269.
157. Capen RL, Latham LP, Wagner WW Jr. Comparison of direct and indirect measurements of pulmonary capillary transit times. *J Appl Physiol* 1987;62:1150–1154.
158. Clough AV, Linehan JH, Dawson C. Regional perfusion parameters from pulmonary microfocal angiograms. *Am J Physiol* 1997;272: H1537–H1548.
159. Clough AV, Haworth ST, Hanger CC, Wang J, Roerig DL, Linehan JH, Dawson CA. Transit time dispersion in the pulmonary arterial tree. *J Appl Physiol* 1998;85:565–574.
160. Hoffman EA, Tajik JK. Dynamic and high resolution CT assessment of pulmonary blood flow distributions. *Am Rev Respir Dis* 1993; 147:A201.
161. Mintun MA, Ter-Pergossian MM, Green MA, Lich LL, Schuster DP. Quantitative measurement of regional pulmonary blood flow with positron emission tomography. *J Appl Physiol* 1986;60:317–326.
162. Tajik JK, Tan BQ, Hoffman EA. CT-based assessment of regional pulmonary blood flow parameters: an update. In: Chen C-T, Clough AV, editors. Medical imaging 1999: physiology and function from multidimensional images; 1999 05/99. San Diego, CA: SPIE; 1999. pp. 181–187.
163. Wolfkiel CJ, Rich S. Analysis of regional pulmonary enhancement in dogs by ultrafast computed tomography. *Invest Radiol* 1992;27:211–216.
164. Bassingthwaighte JB, Raymond GR, Chan JIS. Principles of tracer kinetics. In: Zaret BL, Beller GA, editors. Nuclear cardiology: state of the art and future directions. Mosby: St. Louis, MO; 1993. pp. 3–23.
165. Bentley MD, Lerman LO, Hoffman EA, Fiksen-Olsen MJ, Ritman EL, Romero JC. Measurement of renal perfusion and blood flow with fast computed tomography. *Circ Res* 1994;74:945–951.
166. Eigler NL, Schuhlen H, Whiting JS, Pfaff JM, Zeiher A, Gu S. Digital angiographic impulse response analysis of regional myocardial perfusion: estimation of coronary flow, flow reserve, and distribution volume by compartmental transit time measurement in a canine model. *Circ Res* 1991;68:870–880.
167. Ritman EL. Temporospatial heterogeneity of myocardial perfusion and blood volume in the porcine heart wall. *Ann Biomed Eng* 1998; 26:519–525.
168. Musch G, Layfield JD, Harris RS, Melo MF, Winkler T, Callahan RJ, Fischman AJ, Venegas JG. Topographical distribution of pulmonary perfusion and ventilation, assessed by PET in supine and prone humans. *J Appl Physiol* 2002;93:1841–1851.
169. Levin DL, Chen Q, Zhang M, Edelman RR, Hatabu H. Evaluation of regional pulmonary perfusion using ultrafast magnetic resonance imaging. *Magn Reson Med* 2001;46:166–171.
170. Hatabu H, Tadamura E, Levin DL, Chen Q, Li W, Kim D, Prasad PV, Edelman RR. Quantitative assessment of pulmonary perfusion with dynamic contrast-enhanced MRI. *Magn Reson Med* 1999;42:1033–1038.
171. Hoffman EA, Tajik JK, Kugelmass SD. Matching pulmonary structure and perfusion via combined dynamic multislice CT and thin-slice high-resolution CT. *Comput Med Imaging Graph* 1995;19:101–112.
172. Won C, Chon D, Tajik J, Tran B, Robinswood G, Beck K, Hoffman E. CT-based assessment of regional pulmonary microvascular blood flow parameters. *J Appl Physiol* 2003;94:2483–2493.

173. Schuster DP, Marklin GF. The effect of regional lung injury or alveolar hypoxia on pulmonary blood flow and lung water measured by positron emission tomography. *Am Rev Respir Dis* 1986;133:1037–1042.
174. Osborne DR, Effmann EL, Hedlund LW. Postnatal growth and size of the pulmonary acinus and secondary lobule in man. *AJR Am J Roentgenol* 1983;140:449–454.

APPENDIX

Scan Protocols

Scan protocols together with estimated dose calculations used for these studies are provided in Tables 1 through 3.

Volume Scans

Our current volumetric protocol consists of 100 milliampere-seconds (mAs), 120 kV, and 1-mm collimation, with an effective slice thickness of 1.3 mm, overlap of 0.65 mm, and pitch of 1.2 mm. The slice parameter mode is 32 × 0.6 mm. We will use 512 × 512 slice matrices. The subject is apneic at a controlled lung volume (40 and 95% VC). We carefully check the calibration of the scanner on a weekly basis. To estimate the effective dose, we have used the WinDOSE program developed by Professor Willi Kalender (University of Erlangen, Germany) and the CT dose index (CTDI) for the Siemens Sensation 64. The total effective dose (H_E) is the primary measure that our radiation safety committee evaluates. The radiation dose, as outlined in Table 1**,** from the procedures is equal to the risk that the average American experiences from exposure to 40 months of natural background radiation.

Xenon Regional Ventilation

Reference whole lung scans obtained at static inflations of 40 and 95% VC are used for axial scan locations. A ventilation study is performed at 20 time points with 80 kVp and 150 mAs. The slice parameter mode is 20 × 1.2 mm so that a 2.4 cm (or greater depending on the axial extent of the field-of-view on future scanner configurations) *z*-axis coverage is achieved. To estimate the effective dose, we have used the WinDOSE program and the CTDI for the Siemens Sensation 64. The total effective dose (H_E) is the primary measure that the radiation safety committee evaluates. The radiation dose, as outlined in Table 2, from the procedures is equal to the risk that the average American experiences from exposure to 14 months of natural background radiation.

The ECG signal is replaced by a signal from our custom data acquisition and control program to trigger the scanner at specific points during the ventilatory cycle. The subject breathes spontaneously with a mouthpiece connected to our lung volume controller and two-way switching valve (room air and the Xe Enhancer set to provide 30% Xe/30% O_2). The subject is instructed to maintain a constant breathing pattern by watching a graphical display with target lines. To deliver xenon gas, we use an Enhancer 9000, which allows for xenon recycling. CO_2 is scrubbed from the exhalate and xenon and oxygen are sensed and replaced to maintain a constant concentration of the inspired gas. The scanner is activated via our PC software programmed in the LabView (National Instruments) environment and three gated images are taken as the pre-Xe baseline. The switching valve connects the subject to 30% Xe gas. The subject inhales nine breaths of Xe.

Bolus Contrast Regional Perfusion

Scanning is in the axial mode at the same slice locations as in the ventilation study. To obtain regional perfusion (Q) with contrast injection, the scanner is set up as in the Xe protocols described above, with an ECG trigger signal, and the subject remains apneic during scanning. A Medrad power injector system (Mark V Power Injector; Medrad, Indianola, PA) is used to give a 2-second bolus of contrast (0.5 ml/kg, up to a total volume of 50 ml). The lung volume controller is used to start breath-hold at normal functional residual capacity. Two to three baseline images are obtained followed by dye injection. A total of 12 stacked image sets, one per heartbeat, are obtained to follow the contrast agent (Visipaque; GE Healthcare, Milwaukee, WI) through the lung fields. The scanner is setup in axial, ECG triggering mode, using 80 kVp, 150 mAs, 360° rotations, 0.5-second scan time, 512 × 512 matrix, and the field of view adjusted to fit the lung field of interest. The slice parameter mode is 20 × 1.2 mm so that a 2.4-cm portion of the lung field will be examined. To estimate the effective dose, we used the WinDOSE program and the CTDI for the Siemens Sensation 64. The total effective dose (H_E) is the primary measure that our radiation safety committee evaluates. The radiation dose from the procedures, as outlined in Table 3, is equal to the risk that the average American experiences from exposure to 19 months of natural background radiation.

TABLE 1. RADIATION DOSE ESTIMATES FOR TWO VOLUME SCANS

Volume scans	64 slice	
Two scans	Male	Female
Organs, dose (mrad)		
Lung	2,060	2,100
Breast	0	1,920
Skeleton	1,040	1,200
Esophagus	1,430	1,600
Red marrow	630	680
Skin	3,900	3,900
H_E, mrem	690	1,060

TABLE 2. RADIATION DOSE ESTIMATES FOR VENTILATION STUDY

Ventilation	150 mAs	80 kV
15 scans	Male	Female
Organs, dose (mrad)		
Lung	830	848
Breast	0	900
Skeleton	330	382.5
Esophagus	406	410
Red marrow	150	180
Skin	18,000	18,000
H_E, mrem	236.25	360

TABLE 3. RADIATION DOSE ESTIMATES FOR VENTILATION STUDY

Blood flow	150 mAs	80 kV
20 scans	Male	Female
Organs, dose (mrad)		
Lung	1,320	1,140
Breast	0	960
Skeleton	660	580
Esophagus	540	620
Red marrow	200	240
Skin	24,200	24,200
H_E, mrem	315	480